Evolution of Far-From-Equilibrium Nanostructures Formed by Cluster-Step and Cluster-Cluster Coalescence in Metal Films

C. R. Stoldt, A. M. Cadilhe, C. J. Jenks, J.-M. Wen, J. W. Evans, and P. A. Thiel
Departments of Chemistry and Mathematics, IPRT, and Ames Laboratory, Iowa State University, Ames, Iowa 50011
(Received 14 April 1998)

Scanning tunneling microscopy experiments reveal the formation of a variety of geometrically exotic nanostructures following submonolayer deposition of Ag on Ag(100). These result from the diffusion of large Ag clusters, and their subsequent "collision" and coalescence with extended step edges, and with other clusters. Relaxation of these far-from-equilibrium step-edge configurations is monitored to determine rates for restructuring versus local geometry and feature size. This behavior is analyzed with lattice-gas model simulations to elucidate the underlying atomistic mass transport processes. [S0031-9007(98)07246-9]

PACS numbers: 68.35.Bs, 68.35.Fx, 82.65.Dp

To obtain the most insight into the dynamics of erosion from observations over a limited time span, one would naturally examine the evolution of rugged landscapes rather than smooth terrains. Analogous observations apply to systems studied in physics. The response to *slight* perturbations or spontaneous fluctuations from equilibrium determines macroscopic transport coefficients [1], but the relaxation of systems *far* from equilibrium may provide more insight into underlying transport processes. Such relaxation can reflect a competition between various kinetic pathways, controlled by activation barriers for specific microscopic processes. In this Letter, we study the relaxation of far-from-equilibrium two-dimensional (2D) step-edge nanostructures or "landscapes" on metal surfaces to gain fundamental insight into the atomic-scale processes mediating the approach to equilibrium. This type of study is of relevance to recent intensive efforts to engineer nanostructures [2], which are often surface structures susceptible to rearrangement, in that it constitutes a step towards predicting, and even controlling, their useful lifetime.

One of the more surprising findings of recent scanning tunneling microscopy (STM) studies is that metal surfaces near room temperature, which one might expect to be static, can actually be in a state of flux. This is evidenced by the observed equilibrium fluctuations or "frizziness" of monoatomic step edges on Cu, Au, and Ag surfaces [3]. Evolution of nonequilibrium structures, created either by deposition [4] or by mechanically using the STM tip [5,6], is also observed. Large 2D clusters created by submonolayer deposition of metal(100) homoepitaxial films display unexpected diffusive mobility [7,8]. Cluster diffusion and subsequent coalescence upon collision, rather than Ostwald ripening, can even dominate adlayer coarsening [8,9]. For deposited multilayer Cu/Cu(111) films, diffusion of clusters in higher layers to step edges opens an efficient pathway for downward mass transport, and thus film smoothing [10]. The decay of single layer 2D islands [11,12], as well as of multilayer island stacks [12] and holes [5], has been monitored on Ag(111) and Au(111) surfaces to elucidate associated mass transport processes. All of these are examples of dynamic behavior of metal surface even at room temperature. We note also that sufficiently rapid restructuring of nanostructures influences multilayer film growth [13].

In this Letter, we study the relaxation at 295 K of far-from-equilibrium step-edge nanostructures created by the diffusion and subsequent "collision" and coalescence of 2D Ag clusters with other clusters, and with extended step edges, on an Ag(100) surface (i.e., 2D sintering processes). A comprehensive characterization is provided for varying size, and local geometry of the initial stages of rapid relaxation or restructuring just after collision, where the configuration has a simple geometrical structure due to the near-square shape of islands. Successful, consistent comparison with simulations of a model for adatom diffusion along step edges elucidates the atomistic processes controlling mass transport.

The key experimental details can be described briefly [7,9]. We used an Omicron room temperature STM housed in a UHV chamber with base pressure of below 10^{-10} Torr. Initial film configurations were created by evaporative deposition of Ag onto a single Ag(100) crystal. Large area scans of postdeposition evolution were taken at intervals of 3–15 min, and various examples of cluster diffusion and collision with other clusters and step edges were observed. Rates of change of key dimensions were then monitored, consistently using the FWHM of scan profiles. The database presented here was obtained with various tunneling conditions, and on several single crystals. Its self-consistency indicates that STM tip effects do not significantly influence nanostructure evolution. We focus on four distinct types of events (Fig. 1): collision of clusters with extended step edges of (a) [110], and (b) [100] orientations (these step-edge geometries are shown in Fig. 2); (c) side-to-side, and (d) corner-to-corner collision of pairs of square clusters. [110] is the equilibrium orientation of

 0031-9007/98/81(14)/2950(4)$15.00

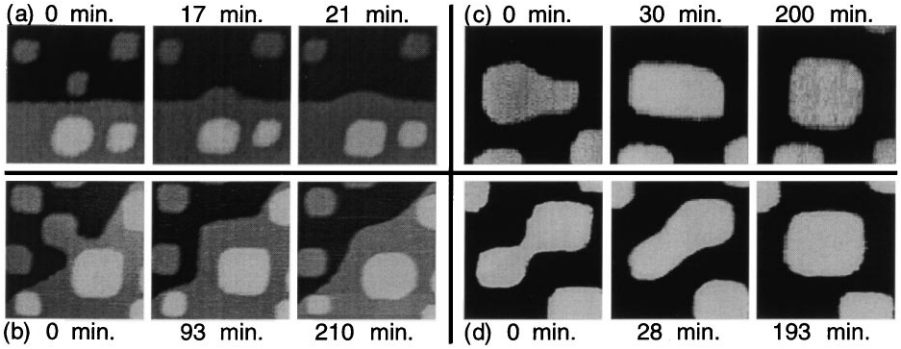

FIG. 1. Coalescence of (a) a cluster and [110] step, with collision at ~10 min (image = 35 × 35 nm^2); (b) a cluster and [100] step (58 × 58 nm^2); (c) a side-to-side cluster pair (35 × 35 nm^2); (d) a corner-to-corner cluster pair (38 × 38 nm^2).

steps, but metastable [100] (and other) orientations result from depositing 0.6–0.8 ML of Ag.

Analysis of the relaxation dynamics rests on key assumptions about the underlying atomistic processes, and of their energetics. First, consider mass transport at step edges mediated by *perimeter diffusion* (PD), wherein atoms hop along the step edge, but do not detach and reattach from it [14,15]. The key processes shown in Fig. 2(a) include fast edge diffusion along straight [110] steps at rate h_e, kink escape at rate h_k, corner rounding at rate h_r, and slow "core breakup" at rate h_c. Corresponding activation barriers are denoted by E_i ($i = e, k, r$, or c), and we assume a common attempt frequency ν. We model the system with *effective* nearest-neighbor (NN) pairwise adatom interactions of magnitude J. Then, the detailed-balance relationship between rates for forward and reverse processes [16] implies that $h_k/h_e = h_c/h_r = \exp[-J/(k_B T)]$. Semiempirical energy calculations for metal(100) homoepitaxy suggest that [14,16] $h_r \approx h_k$, so we choose $E_r \approx E_k = E_e + J$ and $E_c \approx E_e + 2J$.

A goal of this paper is to assess the effective activation barrier, $E_{\rm act}$(PD), for step-edge restructuring. Consider the decay of the rectangular protrusion on a [110] step edge shown in Fig. 2(b). At various stages, it is necessary to disrupt the "rectangular core" of the protrusion, and this requires core breakup. (The same requirement was noted previously for cluster diffusion [7,14].) However, reduction of the height of the protrusion also requires repeated implementation of the *combined process* of kink escape followed by corner rounding [see Fig. 2(b)]. If $\rho_{\rm eq} \approx h_k/h_e = \exp[-J/(k_B T)]$ denotes the quasiequilibrium density of atoms released from the kink site, then this combined process occurs at an effective rate $h_{\rm eff} \approx \rho_{\rm eq} h_r \approx \nu \exp[-(E_r + J)/(k_B T)]$. Thus, both core breakup and the combined process of height reduction yield the same $E_{\rm act}$(PD) $\approx E_e + 2J$. Similar analysis of the decay of a triangular protrusion on a [100] step edge shown in Fig. 2(c) reveals that most of the decay is mediated by core breakup steps, so again $E_{\rm act}$(PD) $\approx E_e + 2J$ $(= E_c)$.

It is appropriate to consider the competing pathway for mass transport via *terrace diffusion* (TD), i.e., detachment and reattachment of atoms from the step edge. The effective barrier for evaporation, and thus for mass transport, is $E_{\rm act}$(TD) $= E_d + 2J$, where E_d denotes the terrace diffusion barrier [17]. For metal(100) homoepitaxy, a reasonable expectation is that [14,16] $E_e \approx E_d/2$. Thus, for Ag/Ag(100) where [18] $E_d \approx 0.40$ eV, one has $E_e \approx 0.2$ eV, and an *energetic advantage* of 0.2 eV for PD over TD. Thus PD should dominate, at least for small-size features and low temperatures. Consequently, the simulation studies described below use a simple lattice-gas model for the PD mechanism incorporating the atomic hops mentioned above, together with a constraint to preserve connectivity of atoms.

We now discuss in detail our experimental observations, and corresponding simulation analyses for the 2D coalescence or sintering processes in Figs. 1(a)–1(d). Below, rates are quoted in terms of the surface lattice constant, $a = 2.89$ Å, for Ag(100).

(a) Cluster + [110] step coalescence [Fig. 1(a)].— Here, the initial configuration is a square protrusion attached edge-on to a straight step. Experimental data indicate a roughly linear variation of the initial rate of decay of the protrusion height with its inverse area, for larger sizes [Fig. 3(a)]. Simulations confirm the equality $E_{\rm act} \approx E_e + 2J$ $(= E_c)$, and match observed rates if $E_{\rm act} = 0.75$ eV (specifically, $E_e = 0.20$ eV, $J = 0.275$ eV, and $\nu = 10^{12}$/s). Both experiment and simulation also show that the decay of a square protrusion does not significantly

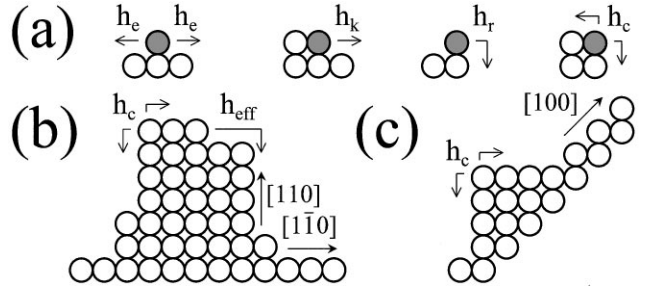

FIG. 2. (a) Key perimeter diffusion processes (see text). Decay of protrusions at (b) [1$\bar{1}$0] (or equivalently [110]), and (c) [100] step edges.

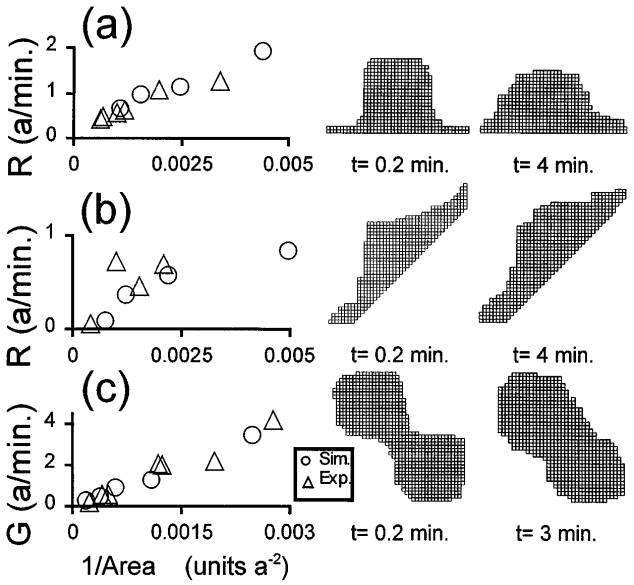

FIG. 3. Decay rate R vs $1/\text{area}$ for the height of (a) square protrusions at [110] step edges, and (b) triangular protrusions at [100] step edges. (c) Neck growth rate G vs $1/(\text{single cluster area})$ for corner-to-corner cluster coalescence. Right insets show simulated configurations.

perturb a perfectly aligned equilibrium [110] step edge, but that steps slightly misaligned from [110] adjust rapidly in the vicinity of the protrusion to achieve the preferred [110] orientation.

(b) Cluster + [100] step coalescence [Fig. 1(b)].—After contact of a cluster corner with the [100] step, both experiment and simulation reveal the *rapid* formation of a connecting meniscuslike neck, together with indentations into the metastable step edge [see Fig. 1(b)]. The rapid neck growth is primarily due to mass flow from the indentations. Simulations reveal an initial fast rise in the neck width with time for about 1 min, followed by more sustained quasilinear growth. For a 50×50 atom cluster, simulations with the above parameters yield a rate of quasilinear growth of 3.1 a/min, and produce a neck width of $35a \approx 100$ Å after about 5 min (a = surface lattice const). These results are entirely consistent with the experimental behavior for the case in Fig. 2(b).

Later, an intermediate configuration of a near perfect right-angled triangle protruding from [100] step develops, the sides selecting the preferred [110] orientations [Fig. 1(b)]. Finally, this triangular protrusion slowly decays. The experimental decay rate of the height at the onset of this final stage is shown in Fig. 3(b) for various triangle sizes. Substantial uncertainties are due to large fluctuations during decay, including wandering and splitting of the protrusion peak. Simulation predictions with the above parameters are consistent with experiment, and show that again $E_{\text{act}} = E_e + 2J$ $(= E_c)$. Decay rates here are far slower than those for square protrusions of the same size at [110] steps. This indicates that mass transport is less efficient along [100] steps than along [110] steps. Presumably, this is because the former requires repeated core breakup steps, whereas the latter requires merely straight edge hopping and kink escape [cf. Figs. 2(b) and 2(c)].

(c) Side-to-side cluster pair coalescence [Fig. 1(c)].—For unequal sized square clusters which collide side-on, rapid mass flow first occurs to fill in the missing corner. This results in significant perimeter length reduction, and some decrease of the long dimension. This mass flow quickly leads to the formation of a long-lived (metastable) near-rectangular shape. The final stage of evolution from the near-rectangular metastable to the near-square equilibrium shape is *much* slower, as seen in both simulation and experiment. The rate of decay of the length is small and difficult to quantify due to significant fluctuations, especially for aspect ratios below about $\frac{3}{2}$ (i.e., close to the equilibrium value of unity).

(d) Corner-to-corner cluster pair coalescence [Fig. 1(d)].—For this configuration, one sees a fairly rapid formation of a meniscuslike neck, analogous to case (b). Neck growth leads to evolution from a dumbbell-shaped to a convex cluster. Subsequent slower evolution produces a near-square equilibrium shape. We focus on neck growth for roughly equal cluster sizes. Simulations again reveal an initial fast rise in the neck width with time, followed by more sustained quasilinear growth. Experimental data in Fig. 3(c) for this rate of quasilinear growth show a roughly linear variation with inverse area of the cluster, for the range of experimental sizes. This behavior is consistently matched by simulations with the above parameters. The rate of quasilinear neck growth of 0.3 a/min for two 50×50 atom clusters is substantially below the rate of 3.1 a/min for the 50×50 atom cluster in case (b) (a = surface lattice const). Clearly, neck growth for dumbbell-shaped clusters via mass transfer from their extremities is less efficient than neck growth via the creation of indentations in a [100] step edge.

In discussing the above results, we first emphasize that our direct STM observations of restructuring for suitably selected far-from-equilibrium nanostructures yield immediate insight into the underlying mass transport processes. The dramatic difference between the rate of decay of protrusions on [110] and [100] step edges reveals a strong dependence of the efficiency of mass transport on step orientation, and thus provides clear evidence for PD-dominated mass transport (since TD should have comparable efficiency for different orientations). This conclusion is supported by our argument for an energetic advantage of PD over TD, by the consistency of our analysis of experimental data with a PD model for very different geometries and sizes, and by the recent demonstration [7] that PD dominates other mass transport mechanisms in controlling the diffusion of 2D Ag clusters on Ag(100). However, the TD and uncorrelated 2D evaporation-condensation (EC) mechanisms of mass transport [7–9] always operate to some degree, in addition to PD, and could dominate

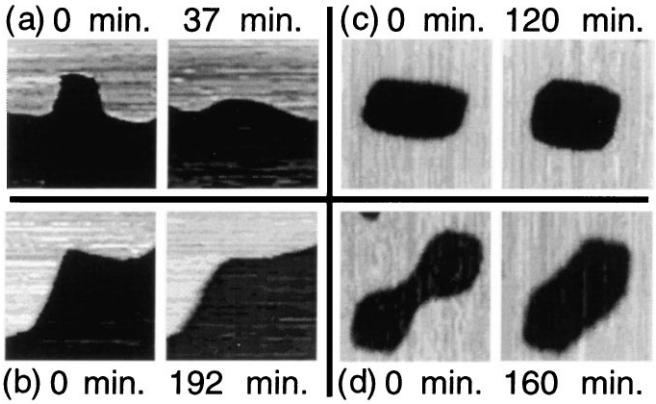

FIG. 4. Vacancy protrusion decay at (a) a [110] step (image = 20×20 nm^2) and (b) a [100] step (50×50 nm^2). Vacancy cluster restructuring for (c) a rectangular shape (45×45 nm^2) and (d) a dumbbell shape (54×54 nm^2).

under different conditions (e.g., higher T, or larger sized structures).

Some aspects of restructuring of the metal surface above seem fluidlike. Hence, it is natural to treat them in a coarse-grained or continuum approach where step-edge evolution is driven by minimization of the step-free energy. Mass flow is proportional to the gradient of a step-chemical potential, which scales with curvature and step-free energy. Simple Mullins-type evolution equations [19] produce slower restructuring with increasing protrusion or cluster area, A, but with rates scaling like $A^{-3/2}$ rather than the observed A^{-1}, for larger A (cf. Fig. 3). Furthermore, continuum treatments cannot assess competition between kinetic pathways, which can strongly influence behavior on the small length scales relevant here. This is most apparent if one considers the complete relaxation process, rather than just the initial restructuring; introducing an "easy" pathway for atoms to round kinks to reach doubly coordinated sites (by concerted exchange with the corner atom), or a lower barrier (below E_c) for single atom diffusion along [100] steps, could significantly influence the kinetics and geometry of the late stage decay of protrusions at step edges.

Another aspect of the modeling involves the adatom interactions, treated here as *effective* NN pairwise interactions of strength $J = 0.275$ eV. Significantly, using such effective interactions to describe the observed transition to reversible island formation during deposition yields a consistent estimate of $J \approx 0.3$ eV [18]. However, a more complicated detailed form for the interactions is likely, so we note that introducing attractive many-body interactions results in a smaller NN dimer pair interaction to fit experimental data.

As a natural extension of the above, we have succeeded in creating almost perfect "mirror images" of the adatom structures in Fig. 1 (i.e., vacancy protrusions into extended step edges, and dumbbell- and rectangular-shaped vacancy clusters), and examined their relaxation. Prolonged deposition on a stepped surface leads to the advance of steps across terraces incorporating islands in the process, and producing an irregular growth structure. These step edges smoothen after deposition stops, occasionally leaving square vacancy protrusions into [110]-like steps [Fig. 4(a)], and triangular vacancy protrusions into [100]-like steps [Fig. 4(b)]. Analysis of limited data for the decay of the depth of protrusions suggests comparable or faster decay rates than for adatom protrusions of the same size, and much higher rates for [110] than [100] steps. Deposition of $\sim$0.8 ML of Ag on large terraces produces irregular gaps between growing islands. These restructure to form more compact vacancies, often with rectangular [Fig. 4(c)] or dumbbell [Fig. 4(d)] shapes. Neck growth for the vacancy dumbbell in Fig. 4(d) is comparable to that for an adatom dumbbell of the same size.

In summary, analysis of the restructuring of exotic far-from-equilibrium step-edge nanostructures in the Ag/Ag(100) system provides direct insight into underlying mass transport processes (and an estimate of 0.75 eV for E_c). The current broad interest in fabrication of far-from-equilibrium nanostructures in surface systems fosters a need for studies like ours to elucidate possible decay mechanisms for such structures.

This work was supported by NSF Grant CHE-9700592, and performed at Ames Laboratory, which is operated for the USDOE by Iowa State University under Contract No. W-7405-Eng-82.

[1] L. Onsager, Phys. Rev. **37**, 405 (1931); **38**, 2265 (1931).
[2] J. A. Stroscio and D. Eigler, Science **29**, 1319 (1991).
[3] M. Giesen-Siebert *et al.,* Phys. Rev. Lett. **71**, 3521 (1993).
[4] Z. Zhang and M. G. Lagally, Science **276**, 377 (1997).
[5] R. C. Jakevic and L. Elie, Phys. Rev. Lett. **60**, 120 (1988).
[6] J. Li *et al.,* Phys. Rev. Lett. **76**, 1888 (1996).
[7] J.-M. Wen *et al.,* Phys. Rev. Lett. **73**, 2591 (1994).
[8] W. W. Pai *et al.,* Phys. Rev. Lett. **79**, 3210 (1997).
[9] J.-M. Wen *et al.,* Phys. Rev. Lett. **76**, 652 (1996).
[10] M. Giesen *et al.,* Phys. Rev. Lett. **80**, 552 (1998).
[11] B. H. Cooper *et al.,* Mater. Res. Soc. Symp. Proc. **280**, 37 (1993).
[12] K. Morgenstern *et al.,* Phys. Rev. Lett. **76**, 2113 (1996).
[13] M. C. Bartelt and J. W. Evans, Phys. Rev. Lett. **75**, 4250 (1995).
[14] A. F. Voter, SPIE **821**, 6819 (1986).
[15] H. Shao, S. Liu, and H. Metiu, Phys. Rev. B **51**, 7827 (1995).
[16] M. Langelaar, Ph.D. thesis (1998); M. Breeman *et al.,* Surf. Sci. **303**, 25 (1993).
[17] If detachment (or bond-breaking) of single atoms at [110] edges has rate h_b, and terrace hopping has rate h_d, then $h_b/h_d = \exp[-J/(k_B T)]$. The effective rate of detachment is $\rho_{eq} h_b$ with ρ_{eq} as in the text.
[18] C.-M. Zhang *et al.,* Surf. Sci. **406**, 178 (1998).
[19] W. W. Mullins, J. Appl. Phys. **30**, 77 (1959).